If the model is to be used in a predictive capacity, the main problems arise in relating the entrainment process through w_e to the calculated turbulent characteristics and in determining whether the predicted structure is likely to remain well mixed. This requires, at minimum, some consideration of the turbulent kinetic energy balance within the boundary layer.

If the model is to be used to aid interpretation of observations it is still useful to diagnose quantities which are actually measured, i.e. $\overline{w'\theta'_v}$ or $\overline{w'q'_t}$.

5.2.1 The buoyancy flux in the stratocumulus-topped boundary layer

The mixed-layer model uses conserved variables. However, the vertical turbulent motions in an cloudy atmosphere are primarily driven by the buoyancy flux $(g/\overline{\theta_v})\overline{w'\theta'_v}$, so it is tempting to derive an expression that relates the fluxes of conserved variables $\overline{w'\theta'_l}$ and $\overline{w'q'_t}$ to the buoyancy flux (or the virtual potential temperature flux $\overline{w'\theta'_v}$). The virtual potential temperature flux in a saturated environment is given by,

$$\overline{w'\theta'_v} = \overline{w'\theta'}(1 + \epsilon_I \overline{q_s} - \overline{q_l}) + \overline{\theta}(\epsilon_I \overline{w'q'_s} - \overline{w'q'_l}), \tag{5.15}$$

where according to Eq. (2.12)

$$\epsilon_I = 1/\epsilon - 1 = R_v/R_d - 1 = 0.61, \tag{5.16}$$

and $\overline{w'q'_s}$ represents the saturated water vapor flux. In the unsaturated subcloud layer all the water is in the vapor phase ($q_l = 0$ and $q_t = q_v$), so in that case the virtual temperature flux reduces to

$$\overline{w'\theta'_v} = \overline{w'\theta'}(1 + \epsilon_I \overline{q_t}) + \overline{\theta}\epsilon_I \overline{w'q'_t}. \tag{5.17}$$

For unsaturated conditions we also have that the liquid water potential temperature flux reduces to the potential temperature flux $\overline{w'\theta'_l} = \overline{w'\theta'} - (L_v/c_p)\overline{w'q'_l} = \overline{w'\theta'}$. Thus, for an unsaturated atmosphere the virtual potential temperature flux in terms of conserved variables reads

$$\overline{w'\theta'_v} = \overline{w'\theta'_l}(1 + \epsilon_I \overline{q_v}) + \overline{\theta}\epsilon_I \overline{w'q'_t} = A_d \overline{w'\theta'_l} + B_d \overline{w'q'_t}, \tag{5.18}$$

by which we have defined the coefficient $A_d \approx 1.01$ and $B_d \approx 170$ for dry convection.

For the cloud layer the derivation is less straightforward. With aid of Eq. (5.16) and using that $q_t = q_s + q_l$ we can write

$$\epsilon_I q_s - q_l = (1 + \epsilon_I)q_s - q_t = \frac{q_s}{\epsilon} - q_t. \tag{5.19}$$

Using this expression we can rewrite Eq. (5.15):

$$\overline{w'\theta'_v} = \overline{w'\theta'}(1 + \frac{\overline{q_s}}{\epsilon} - \overline{q_t}) + \overline{\theta}(\frac{\overline{w'q'_s}}{\epsilon} - \overline{w'q'_t}). \tag{5.20}$$

The Clausius-Clapeyron equation (1.55) can be expressed in terms of the saturation specific humidity,

$$\frac{dq_s}{dT} = \frac{q_s l_v}{R_v T^2}. \tag{5.21}$$

If we write $dq_s = q'_s$ and $dT = T'$ then saturation specific humidity fluctuations are uniquely related to perturbations in the temperature,

$$q'_s = \frac{q_s l_v}{R_v T^2} T' \qquad \Longleftrightarrow \qquad q'_s = \left(\frac{dq_s}{dT}\right) T'. \tag{5.22}$$

This facilitates to write the saturation specific humidity flux as a (potential) temperature flux,

$$\overline{w'q'_s} = \left(\frac{dq_s}{dT}\right) \overline{w'T'} \approx \left(\frac{dq_s}{dT}\right) \overline{w'\theta'}, \tag{5.23}$$

where the error in the last approximation is less then a few percent. No we can substitute $\overline{w'q'_s}$ out of (5.20) to obtain

$$\overline{w'\theta'_v} = \overline{w'\theta'} \left[1 + \frac{\overline{q_s}}{\epsilon} - \overline{q_t} + \frac{\overline{\theta}}{\epsilon}\left(\frac{dq_s}{dT}\right)\right] - \overline{\theta}\overline{w'q'_t}. \tag{5.24}$$

Next, we use $\overline{w'\theta'} = \overline{w'\theta'_l} + (L_v/c_p)\overline{w'q'_l}$ to give

$$\begin{aligned} \overline{w'\theta'_v} = {} & \overline{w'\theta'_l} \left[1 + \frac{\overline{q_s}}{\epsilon} - \overline{q_t} + \frac{\overline{\theta}}{\epsilon}\left(\frac{dq_s}{dT}\right)\right] \\ & + \overline{w'q'_l}\left(\frac{L_v}{c_p}\right)\left[1 + \frac{\overline{q_s}}{\epsilon} - \overline{q_t} + \frac{\overline{\theta}}{\epsilon}\left(\frac{dq_s}{dT}\right)\right] - \overline{\theta}\overline{w'q'_t}. \end{aligned} \tag{5.25}$$

Last, we would like to substitute out the liquid water flux $\overline{w'q'_l}$. To this end we write

$$\begin{aligned} \overline{w'q'_l} &= \overline{w'q'_t} - \overline{w'q'_s} = \overline{w'q'_t} - \left(\frac{dq_s}{dT}\right)\overline{w'\theta'} \\ &= \overline{w'q'_t} - \left(\frac{dq_s}{dT}\right)\left[\overline{w'\theta'_l} + \left(\frac{L_v}{c_p}\right)\overline{w'q'_l}\right], \end{aligned} \tag{5.26}$$

which yields for $\overline{w'q'_l}$

$$\overline{w'q'_l} = \frac{\overline{w'q'_t}}{1 + \frac{L_v}{c_p}\left(\frac{dq_s}{dT}\right)} - \frac{\overline{w'\theta'_l}\left(\frac{dq_s}{dT}\right)}{1 + \frac{L_v}{c_p}\left(\frac{dq_s}{dT}\right)}. \tag{5.27}$$

The final expression for the virtual potential temperature flux in a saturated atmosphere is then given by

$$\overline{w'\theta_v'} = A_w \overline{w'\theta_l'} + B_w \overline{w'q_t'}, \tag{5.28}$$

with coefficients A_w and B_w having a weak temperature dependency,

$$A_w = \frac{1 + \frac{\overline{q_s}}{\epsilon} - \overline{q_t} + \frac{\overline{\theta}}{\epsilon}\left(\frac{dq_s}{dT}\right)}{1 + \frac{L_v}{c_p}\left(\frac{dq_s}{dT}\right)} \approx 0.5, \tag{5.29}$$

and

$$B_w = A_w \left(\frac{L_v}{c_p}\right) - \overline{\theta} \approx 1100. \tag{5.30}$$

In summary, from Eqs. (5.12) and (5.13) we can obtain the vertical fluxes for q_t and θ_l, respectively. Given these fluxes, the buoyancy fluxes in the subcloud and cloud layer follow straightforwardly from Eqs. (5.18) and (5.28), respectively.

With the mixed-layer model we are capable to address the following questions:

• How does the buoyancy flux profile in the stratocumulus-topped boundary layer look like?

• Turbulent eddies are capable to penetrate into the inversion layer and mix free atmosphere air into the boundary layer. One may intuitively argue that more buoyancy production of turbulent kinetic energy will support more entrainment. Is this indeed the case?

• What is cloud-top entrainment instability?

• Sometimes a two-layer turbulence structure is found in the stratocumulus-topped boundary layer. During the day this is often due to cloud warming by the absorption of shortwave radiation which can lead to a local stable stratification near the cloud base. How can we explain a decoupling between the subcloud and cloud layer during the night?

5.3 Results from a mixed-layer model

We computed flux profiles for nocturnal stratocumulus with the mixed-layer model for different entrainment rates. The boundary conditions are displayed in Table 5.1. During the night there is no solar radiation, and the longwave radiation profile is based on Figure 4.5, with $F_3 = 70$ W/m^2 and linearly decreasing to a zero net radiative flux over a downward vertical distance of 30 m ($F = 0$ W/m^2 for $z < z_i - 30$m).

Figure 5.2 shows that the total water flux is linear with height. For all entrainment rates shown, the flux gradient is positive indicating that for the examples

Parameter	value	units
$\overline{w'\theta'_{l0}}$	0.0033	mKs^{-1}
$\overline{w'q'_{t0}}$	0.007	ms^{-1}(g kg^{-1})
$\Delta\overline{\theta_l}$	6.2	K
$\Delta\overline{q_t}$	-1.2	g kg^{-1}
cloud base	240	m
cloud top	755	m

Table 5.1: Boundary conditions used for the mixed-layer model.

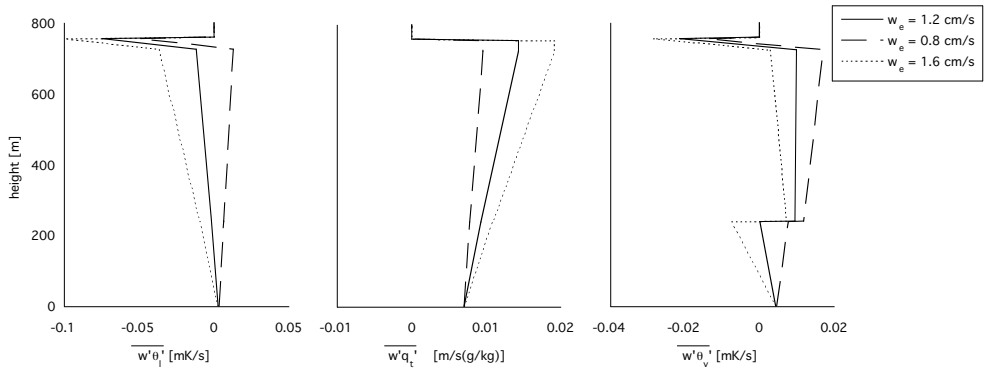

Figure 5.2: Vertical flux profiles computed with a mixed-layer model. Shown are $\overline{w'\theta'_l}$ (left panel), $\overline{w'q'_t}$ (middle panel) and $\overline{w'\theta'_v}$ (right panel). The three lines indicate results obtained for different entrainment rates, 0.8 (dashed line), 1.2 (solid line) and 1.6 (dotted line) cms^{-1}, respectively.

shown entrainment drying exceeds the turbulent flux of moisture from the surface. The case with the largest entrainment rate has the largest drying rate of the boundary layer. The liquid water potential temperature flux has a sharp jump at the boundary-layer top due the longwave radiative flux divergence; below this radiatively cooled layer the flux is linear with height.

Most particular is the shape of the virtual potential temperature flux profile. Because the fluxes of q_t and θ_l are continuous near the cloud base the jump of $\overline{w'\theta'_v}$ must be due to the different coefficients used in Eqs. (5.18) and (5.28). Because $A_w < A_d$ and $B_w > B_d$, the positive values for $\overline{w'\theta'_v}$ are predominantly due to latent heat release effects incorporated in the total water flux. Although at the top of the boundary layer $\overline{w'\theta'_v} < 0$ by entrainment of warm air, the entrainment warming is more than compensated by the longwave radiative cooling as just below the radiatively cooled layer the virtual potential temperature flux is positive.

It is interesting to note that smaller values for $\overline{w'\theta'_v}$ are associated with larger entrainment rates. The interpretation is that more entrainment leads to more downward mixing ($w' < 0$) of warm air ($\theta'_v > 0$) which tends to diminish the buoyancy flux.

Last, a careful inspection of magnitude of the virtual potential temperature flux below the cloud base shows that it can become negative. This implies that at the top of the subcloud layer the upward motions of the relatively moist thermals driven from the surface are damped. If the virtual potential temperature flux is sufficiently negative, the thermals may not be capable anymore to penetrate into the cloud layer. In that case the transport from moisture from the surface into the cloud layer is significantly reduced or even cut off, a situation which is referred to as decoupling. Because entrainment continues to mix in warm and dry air from above, decoupling can lead to a rapid thinning of the cloud layer.

5.3.1 Buoyancy reversal

The virtual potential temperature flux at the top of the cloud layer can be written as

$$\overline{w'\theta'_{vT}} = A_w\overline{w'\theta'_{lT}} + B_w\overline{w'q'_{tT}} = -w_e(A_w\Delta\overline{\theta_l} + B_w\Delta\overline{q_t}), \tag{5.31}$$

where we used the entrainment-jump relation (5.5). If

$$\Delta\overline{\theta_l} < -\frac{B_w}{A_w}\Delta\overline{q_t} \tag{5.32}$$

the virtual potential temperature flux due to entrainment becomes positive, $\overline{w'\theta'_{vT}} > 0$. For $\Delta\overline{q_t}$ in g/kg, $B_w/A_w \approx 2.2$. The physical interpretation of this finding is as follows. If warm and dry air from above the inversion is entrained and subsequently mixed into the cloud layer, the mixed parcel will experience some cooling

due to the evaporation of cloud droplets. Under certain conditions, the cooling will more than compensate the warming due to entrainment, and as a result the mixed parcel will become negatively buoyant with respect to its environment, which is referred to as *buoyancy reversal*. Because a negatively buoyant parcel will have a higher density with respect to its environment, it will sink and generate turbulent kinetic energy, promoting further entrainment. This process is called *cloud-top entrainment instability* (CTEI). It has been suggested that CTEI can lead to a rapid dissipation of stratocumulus, or, that it might be important in the transition from stratocumulus to cumulus (Randall, 1980; Deardorff, 1980).

Several CTEI criteria have been proposed in the literature based on different physical assumptions or from a laboratory study. Nevertheless, none of the proposed CTEI criteria has been generally accepted as being a mechanism responsible for stratocumulus break-up. On the contrary, Kuo and Schubert (1988) analyzed rawinsonde soundings presented in the literature to evaluate the CTEI criterion (5.32), and the effects of CTEI on cloud amount, and concluded that stratocumulus can persist for extended periods, even though the CTEI criterion was satisfied.

5.4 Entrainment

From the analysis with the mixed-layer model it is clear that the entrainment fluxes of heat and moisture play a major role in determining the evolution of the cloud layer. From this perspective it is rather unfortunate that there are only a few measurements available of the entrainment rate in stratocumulus clouds. There are a few different approaches possible to estimate the entrainment rate from observations.

First, we could use observations of the temporal evolution of the cloud-top height (z_i) from remote-sensing devices or tethered-balloon observations, and utilize Eq. (5.6), which is repeated here for convenience,

$$\frac{dz_i}{dt} = w_e + \overline{w}.$$

As an example, Figure 5.3 displays the inversion height which approximately corresponds to the cloud-top height. If one would have information of the subsidence rate Eq. (eq:zi) would then straightforwardly give the entrainment rate. The difficulty of this approach is that the large-scale subsidence $\overline{w}$ at cloud top is on the order of 1 cms^{-1} and hard to measure, although some researchers have used the horizontal wind velocities from observations like radiosondes to estimate $\overline{w}$ from the continuity equation ($\partial\overline{w}/\partial z = -(\partial\overline{u}/\partial x + \partial\overline{v}/\partial y)$. Otherwise, estimations for

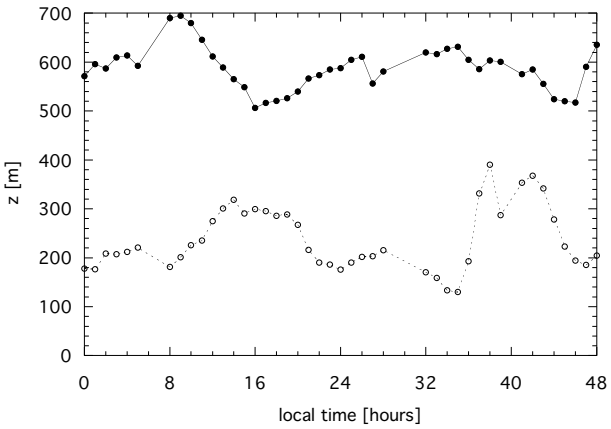

Figure 5.3: The cloud-base (open circles connected by the dashed line) and cloud-top height (filled circles and solid line) from observations as a function of time for 14 and 15 July 1987 (denoted from 0 to 48 hours Local Time). The plot symbols are according to the legend. Cloud-base height was measured by a Väisälä CT 12K laser ceilometer and a sodar was used to estimate the inversion height capping the cloud top. These instruments were operated on San Nicolas island, approximately $33°15'N$ and $119°30'W$, to monitor cloud properties with a high temporal resolution. The cloud layer depth shows a distinct diurnal cycle. During the night the cloud layer becomes thicker, but during the day there is a gradual thinning due to cloud warming by the aborption of solar radiation.

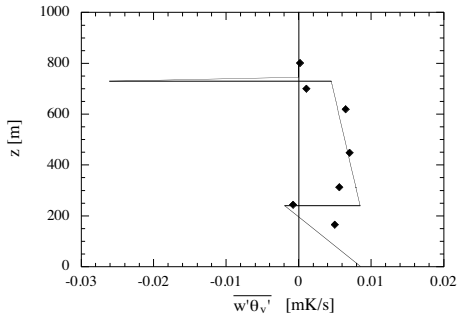

Figure 5.4: Aircraft observations of the virtual potential temperature flux (black diamonds) in a stratocumulus-topped boundary layer over the Atlantic Ocean during ASTEX. The mixed-layer model was utilized to estimate the entrainment rate by fitting the computed virtual potential temperature flux (solid line) to the observations. For this case an entrainment rate of 0.93 cms^{-1} was found. *From Duynkerke et al. (1995).*

$\overline{w}$ may be taken from General-Circulation Models, although the modeled large-scale vertical velocity fields do sometimes exhibit unphysical oscillations which casts some doubt on its accuracy. Also note that the inversion height may change by large-scale horizontal advection, provided the presence of a large-scale horizontal gradient in the inversion height.

Second, aircraft observations of turbulent fluxes of conserved variables at different heights can be used. If it is assumed that the boundary layer is in a quasi-steady state, the fluxes will be linear and the flux just below cloud top can be extrapolated from the observations. If the jump across the inversion is measured, the flux-jump relation ($w_e = -\overline{w'\psi'}_T/\Delta\overline{\psi}$) can be applied. The quantity ψ may be the total specific humidity, ozone, or dimethyl sulfide (DMS). In principle, with aid of Eq. (5.13) this approach can also be used for θ_l or θ_e, but this requires to take the radiative flux divergence into account.

Third, one can do a budget study by analysis of the variation with time for mean quantities in the boundary layer. In the absence of sources and sinks, the tendencies are controlled only by the surface and entrainment fluxes.

Last, given observations of the buoyancy flux, the mixed-layer model can be used as a diagnostic tool to estimate the entrainment rate. If measurements are available of the radiation profile and the boundary conditions similar to the quantities shown in Table 5.1 one can fit the mixed-layer model buoyancy flux profile to the observations. Figure 5.4 gives an example of this approach.

In the following we will explore whether similarity relationships for the clear

convective boundary layer (CBL) can be applied to stratocumulus. In the CBL the virtual potential temperature flux is linear with height (see Figure 4.7), and its value at the top of the mixed layer is approximately a constant fraction $A \approx 0.2$ of the surface flux,

$$\overline{w'\theta'_{vT}} = -w_e \Delta\overline{\theta_v} = -A\overline{w'\theta'_{v0}}, \tag{5.33}$$

where we used the flux-jump relation (5.5). The convective scaling velocity w_* gives a measure of the buoyancy flux production of turbulent kinetic energy and is defined as

$$w_* = \left[2.5\frac{g}{\theta_0}\int_0^{z_i} \overline{w'\theta'_v} dz\right]^{1/3}. \tag{5.34}$$

Note that for $A = 0.2$ the factor 2.5 in Eq. (5.34) cancels if one computes the integral with the flux at the top given by (5.33) :

$$w_*^3 = 2.5\frac{g}{\theta_0}\int_0^{z_i}\left[\overline{w'\theta'_{v0}}(1-\frac{z}{z_i}) + \overline{w'\theta'_{vT}}\frac{z}{z_i}\right] dz = \frac{g}{\theta_0}\overline{w'\theta'_{v0}} z_i. \tag{5.35}$$

By defining a Richardson number Ri_{w_*} for convectively driven layers,

$$Ri_{w_*} = \frac{g z_i}{\theta_0}\frac{\Delta\overline{\theta_v}}{w_*^2}, \tag{5.36}$$

we can express a scaling relation for the entrainment rate

$$\frac{w_e}{w_*} = A Ri_{w_*}^{-1}. \tag{5.37}$$

This formula predicts the entrainment rate in the CBL, and it is interesting to see whether it may also be applied to stratocumulus. Entrainment rates have been determined on the basis of observations made by aircraft in stratocumulus over the North Sea and the Atlantic Ocean. The latter case was part of ASTEX (Atlantic Stratocumulus to Cumulus Transition Experiment), a large field experiment dedicated to the study the transition of stratocumulus to cumulus in the Hadley circulation. Figure 5.5 shows systematic larger values for the entrainment rate in stratocumulus which suggests that the entrainment rate is larger than in the CBL.

Entrainment rate parametrizations often include the convective velocity scale w_* as measure of the buoyancy forcing. Scaling the entrainment rate in stratocumulus is complicated not only because the buoyancy flux depends on the entrainment rate, but also since the number of free parameters that determine the vertical profile of the buoyancy flux is much larger than that for the dry convective boundary layer. In the latter case, the entrainment rate is proportional to

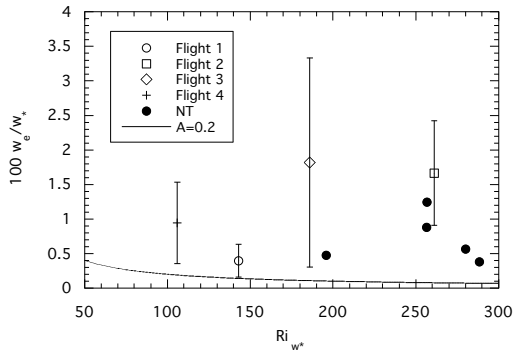

Figure 5.5: Flux-derived entrainment rates with error bars as a function of the convective Richardson number Ri_{w_*} for Flights 1-4 from the ASTEX First Lagrangian. Also plotted are aircraft-derived entrainment rates by Nicholls and Turton (1986) ('NT') and the scaling relation for the entrainment in the clear convective boundary layer, Eq. (5.37) with $A = 0.2$. Symbols and lines are according to the legend. *From De Roode and Duynkerke (1997).*

the ratio of the surface buoyancy flux $\overline{w'\theta'_v}_0$ and the buoyancy jump across the inversion $\Delta\theta_v$. However, according to Eq. (5.28) the total water flux gives a large contribution to the buoyancy flux in a stratocumulus cloud layer, which is due to the condensation and evaporation of liquid water droplets. For this reason, the surface moisture flux, the total specific humidity jump across the inversion, the cloud-base and cloud-top heights, and the long-wave radiative flux divergence at the cloud top (ΔF_l) are all relevant quantities. In summary, if we assume that the entrainment rate depends on the vertical profile of the buoyancy flux, a general scaling expression will depend on the following quantities

$$w_e = f(\overline{w'\theta'_v}(z)) = f(\overline{w'\theta'_l}_0, \overline{w'q'}_0, \Delta\theta_l, \Delta q_t, c_b, c_t, \Delta F_l). \tag{5.38}$$

In addition, short-wave radiative absorption in the cloud layer during daytime, windshear, and drizzle also affect the buoyancy flux profile. The sensitivity of the buoyancy flux to the quantities summarized above, and the role of the entrainment rate on the buoyancy flux vertical profile can all be clearly illustrated by means of a mixed layer model.